JSEE Vol. 27, No. 1, 2025 DOI: 10.48303/jsee.2024.2031989.1100

Research Paper

The Cyclic Behavior Assessment for Equipped Frames with the Novel Load-Resisting System: Eccentric-Braced Frames with Steel Shear Plate Infills

Reza Khalili Sarbangoli[1], Ahmad Maleki[2*] and Ramin K. Badri[3]

1. Ph.D. Student, Department of Civil Engineering, Maragheh Branch, Islamic Azad University, Maragheh, Iran
2. Assistant Professor, Department of Civil Engineering, Maragheh Branch, Islamic Azad University, Maragheh, Iran
*Corresponding Author; email: ad.maleki@iau.ac.ir
3. Assistant Professor, Department of Civil Engineering, Azarshahr Branch, Islamic Azad University, Azarshahr, Iran

Received: 11/06/2024
Revised: 06/08/2024
Accepted: 21/08/2024

Keywords:
Steel frame; Eccentric brace; Stiffener; Finite element; Cyclic loading; Energy dissipation; Stiffness

ABSTRACT

One of the important advantages of steel plate shear walls (SPSWs) is the possibility of creating openings with various geometric dimensions and in different positions on the steel plate. The goal is to offer a novel kind of steel shear walls with an eccentric brace and enhance the system's seismic behavior by including a brace at the opening edges. To evaluate the perf-ormance of the proposed frames, a finite element analysis was used, considering the nonlinear parameters of materials and geometry under cyclic loading. The findings of the numerical models reveal that transforming the infill plate's surface into regular and smaller geometric forms causes the plate's buckling mode. Moreover, the extension of the braces and their connection to the bottom of the beam creates diagonal tension fields in the plate and prevents local buckling of the plate at the opening edge.

How to cite the article:
Khalili Sarbangoli, R., Maleki, A., & Badri, R. K. (2025). The Cyclic Behavior Assessment for Equipped Frames with the Novel Load-Resisting System: Eccentric-Braced Frames with Steel Shear Plate Infills. *Journal of Seismology and Earthquake Engineering*, *27*(1), 57-71. doi: 10.48303/jsee.2024.2031989.1100

1. Introduction

Recent studies have demonstrated that these systems exhibit high resistance, appropriate energy dissipation, and stiffness against lateral forces. Due to their simplicity in execution, their use has rapidly expanded. Consequently, in recent decades, SPSWs have been employed to construct, reinforce, and retrofit structures in highly seismic countries (Farzampour et al., 2015), (Jin and Bai, 2019). One of the critical design issues of structures, especially in high seismic hazard regions, is to control the displacement under earthquake lateral loads. SPSWs are usually considered lateral load-resisting systems to improve the seismic behavior of structures (Dubina and Dinu, 2014; Ghosh and Kharmale, 2010; Pachideh et al. 2019), SPSWs consist of steel plates encompassed by columns and beams. These steel plates are susceptible to buckling in the zone of diagonal compression (Sahoo et al., 2015). SPSWs have been typically utilized to add stiffness to high-rise structures. The simplified model is often used instead of complex models to predict the lateral strength of diagonally stiffened SPSWs (DS-SPSWs), e.g., the simplified cross-brace strip model (CBSM). To predict the lateral strength of diagonally stiffened SPSWs (DS-SPSWs), the simplified cross-brace strip model (CBSM) is proposed. Furthermore, a modification factor is proposed to calculate the shear action of thin steel plates. The CBSM shows good agreement with theoretical calculations. Compared to the DS-SPSW test results, the errors associated with the CBSM are below 5.67% (Yang et al., 2022). A new type of SPSWs with concentric rings was proposed to solve the problem of premature buckling at low drifts. The numerical models and the reduction of capacity up to a drift of 6% are not observed (Farrokhi et al., 2022). Nassernia and Showkati (2017) examined the theoretical and experimental aspects of a specific type of shear wall with a circular opening in the middle span, braced by tension braces connected to the side frame. The implementation of an intermediate shear wall aims to avoid the need to reinforce the primary columns. In their study, the steel plate was attached to a rigid frame. A laboratory-scale system measuring 80 cm was constructed and subjected to cyclic loading. The results indicated that using tension braces with flexural resistance reduces out-of-plane buckling under lateral loading. Furthermore, the presence of an opening in the middle of the steel plate decreases its stiffness and capacity, with the reduction directly related to the diameter of the opening (Nassernia and Showkati, 2017). Numerous studies have shown that implementing steel shear walls improves structural ductility, stiffness, and ultimate strength. In these structures, the connection of the steel plate to boundary elements plays a crucial role in the overall performance of the structure. The standard connection of infill shear plates to boundary elements with a constant surface area is suitable for general construction. In a study by Paslar et al. (2020), the connection of infill plates to boundary elements was examined by creating 57 computational models, following the validation of the computational modeling method. The structural performance of semi-connected plates with various commonly used intermediate connections was evaluated and compared to fully connected infill plate systems. According to the results of these models, it was observed that in shear walls connected only to beams, the capacity and resistance to lateral loads were significantly higher than in plates connected only to columns, due to the limitation of the development of the diagonal tension field.

Additionally, with an 80 percent connection between the infill plate and boundary elements, the system achieved at least 98.9 percent of the ultimate lateral resistance, 96.5 percent of the stiffness, 97.6 percent of the ductility, and 98.6 percent of the energy dissipation capacity of a fully connected steel shear wall system (Paslar et al., 2020).

A novel steel plate shear wall (SPSW) design incorporates inclined stiffeners as tension field guides. These stiffeners are added at the corners of the shear wall, along with an intermediate link beam similar to those in eccentrically braced frames (EBFs). The addition of diagonal members results in a system that combines the features of SPSWs with those of EBFs. In the proposed system, the diagonal stiffeners can alter the tension field pattern, transferring plastic stresses from the column to the link beam. Consequently, the failure mechanism of the system consists of a two-stage flexible fuse mechanism: the yielding of the steel plate in tension and the formation of bending stresses

or plastic shear hinges at the ends of the link beam. Fuses in the unstiffened steel shear wall dissipate more energy than those in the proposed shear wall (Es et al., 2023). Based on the demand for high-performance systems and lateral resistance for tall buildings, a new SPSW structure featuring low-yield-point stiffeners with greater bending rigidity in a T-shaped configuration was proposed. The results showed that T-shaped stiffeners significantly enhance energy dissipation capacity, while T-shaped diagonal stiffeners have the most significant impact on increasing load-bearing capacity (Wang et al., 2024). Our computational findings highlight the advantages of adopting SPSW panels for lateral load resistance. These panels offer greater stiffness, ultimate strength, ductility, and energy dissipation compared to conventional braced frames (CBF). The yield and maximum force applied to SPSP are significantly higher than those of CBF, with ductility and displacement values of SPSP being notably higher than those of CBF (Ras & Basri, 2024). Zarrinkolaei et al. (2021) conducted a parametric study to investigate the effects of circular and oval openings in the shear wall panel. They examined the arrangement, layout, and number of openings on the structural behavior regarding energy absorption, load-bearing capacity, and stress distribution in the steel plate. Finite element (FE) model results under cyclic loading showed a significant decrease in shear capacity and energy absorption (on average 20%) with an increase in opening area. Furthermore, models with horizontal oval holes generally demonstrated the highest shear capacity compared to those with circular openings. Thin corrugated steel plates serve as elements for transferring lateral forces to structural systems. Roudsari et al. (Roudsari et al., 2021) investigated the effects of openings at specific locations in shear wall systems. The study considered corrugated and rectangular steel plates of two different thicknesses with square and circular openings. The performance of steel shear walls concerning the opening location was also examined. Results indicated that increasing the thickness of the corrugated steel plate increases load-bearing capacity. Additionally, a square opening reduces the shear wall's load-bearing capacity more than a circular opening. In shear walls without openings, trapezoidal plates have greater capacity under lateral load compared to corrugated plates.

One advantage of braces is the increase in system rigidity and control over the lateral displacement of the structure. However, increased structural rigidity reduces ductility and the earthquake energy absorption capacity. Steel shear walls not only offer high rigidity but also possess suitable ductility and energy dissipation capacity. In shear wall systems, structural stability is significantly enhanced compared to that of eccentrically braced frames. Therefore, this study aims to achieve both parameters-ensuring flexibility and strength while reducing architectural limitations-by using infill plates between beams, columns, and braces, with openings provided between braces to access the space on both sides of the wall.

2. Equation

US Steel Code (AISC, 2016) was used to design SPSWs. In this code, the dimensions of the beam and the column are determined based on the initial values of loads. The steel plate is then designed similarly to a truss member under the tensile load. Then, the thickness of the steel plate is calculated according to Equation (1):

$$t = \frac{2A_b\,\Omega\,\sin\theta}{L\sin 2a} \tag{1}$$

where A_b is the equivalent brace cross-section, Ω is by section F5 of clause 8, which is 1.2 for the steel shear wall structure. θ is the assumed angle of inclination of the tension field measured from the vertical, L is the width of the frame span, $2a$ is the double of the angle of the diagonal tension field and I_C is a minimum moment of inertia (I_C). Thus, to determine this angle (a), we use Equation (2):

$$an^4 a = \frac{1+\dfrac{t.L}{2A_c}}{1+th\left(\dfrac{1}{A_g}+\dfrac{h^3}{360I_cL}\right)} \tag{2}$$

In Equation (2), A_C represents the cross-sectional area of the columns, and I_C is the moment of inertia of the columns connected to the SPSW. h and A_g are the story height and the beam's cross-sectional area, respectively. The equivalent cross-sectional area of the brace is determined to specify the

thickness of the plate, and then the thickness of the plate is specified based on the total cross-sectional area of the brace. In this method, the plate is converted into several diagonal strips, and Equation (3) determines the cross-sectional area of each strip.

$$A_c = \frac{L\cos a + h\sin a}{n} t \quad (3)$$

Additionally, to prevent the buckling of vertical boundary elements due to the influence of the diagonal tension field, the minimum moment of inertia of the vertical boundary elements must comply with Equation (4):

$$I_c \geq \frac{0.00307 t h^4}{L} \quad (4)$$

3. Numerical Modeling

3.1. Numerical Validation

Sigariyazd et al. analyzed SPSW structures with diagonal stiffeners (Sigariyazd et al. 2016). The SPW-0 sample, which is shown in Figure (1), is used to verify the proposed numerical model. The sample consists of an SPSW without any stiffeners. The model is pushed statically to observe the nonlinear phase of behavior. According to Figure (2), a good correlation is observed among the results of the numerical and laboratory models, and the ...maximum difference between the two diagrams is about 7%. In Figure (2), at a displacement of 3.8 mm, a jump in the structure is observed. This jump occurs in the elastic region of behavior, and the steel plates buckle when they reach the allowable load limit. Before reaching this limit,

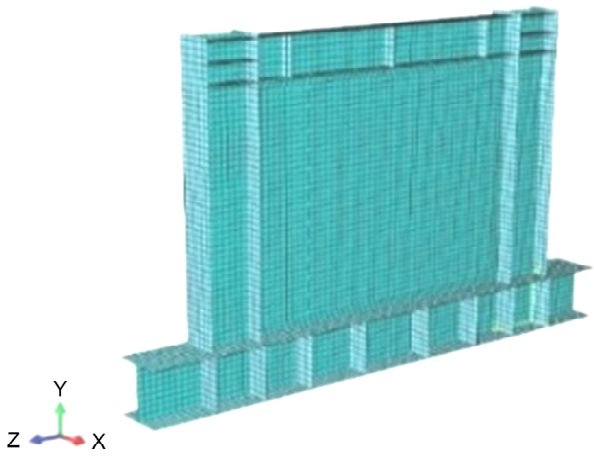

Figure 1. Finite element model.

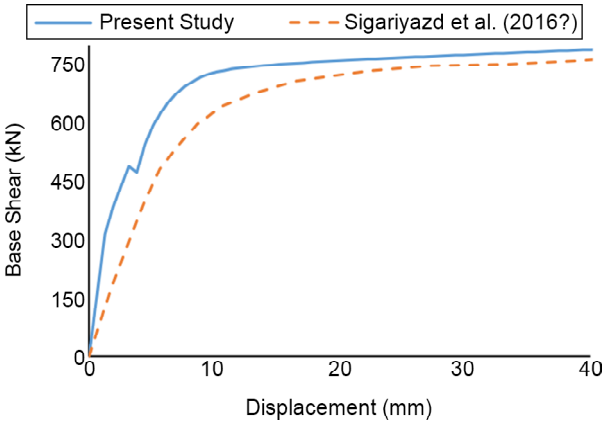

Figure 2. Comparison of laboratory results with finite element model.

initial diagonal tension fields form, causing sudden jumps in the structural response. This phenomenon does not imply systematic instability. As the load continues, the system reaches a new equilibrium with geometric deformation, simultaneously transitioning from in-plane shear to diagonal tension. As shown in Figure (2), the system reaches equilibrium with a new geometric deformation, and after the jump, the system's stiffness increases with the load increment.

For the verification of SPSWs under cyclic loading, the one-bay, three-story model by Wang et al. (Figure 3) was used (Wang et al., 2015). To account for construction imperfections, an out-of-plane displacement was considered in the middle of the infill plate (6.7 mm for the first floor, 8.8 mm for the second floor, and 26 mm for the third floor). In Figure (3), the stress contour for the numerical model is shown. Figure (4) presents

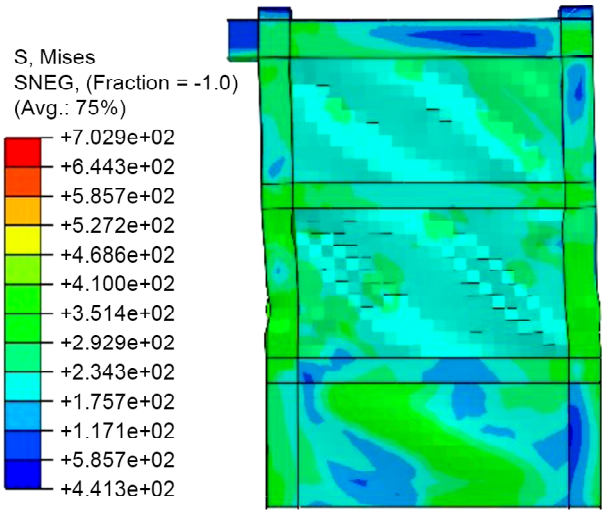

Figure 3. Numerical stress contour for Wang et al. (2015) models.

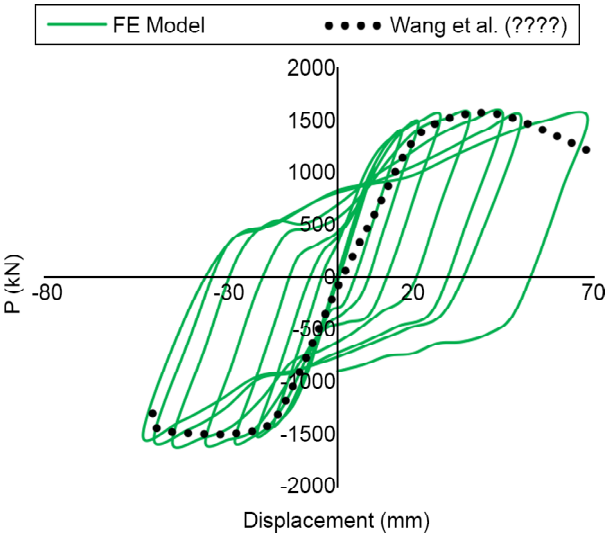

Figure 4. Numerical versus experimental results for Wang et al. (2015).

the experimental model's envelope alongside the cyclic output of the FE model. The maximum base shear in the numerical model is 1571 kN; in the experimental model, it is 1493 kN, with a difference of 4.96%. The difference in the area under the envelope of the experimental and numerical models is approximately 9.5%.

Several laboratory models related to the proposed topic should be examined using finite element software to ensure the accuracy of the modeling methods. Due to the absence of comprehensive experimental models, various verification analyses are used to cover this lack of knowledge. The model presented by Berman and Bruneau (2007) is utilized to investigate the behavior of eccentric braces, as shown in Figure (5). According to Figure (6), at the inflection point, the maximum response for the experimental model is 561 kN, and for the numerical model, it is 580 kN, with a maximum difference of 3.4%. There is a good agreement between the experimental and numerical models in the elastic and plastic regions after the inflection point.

A four-node shell element S4R with reduced integral is used to avoid shear locking. Assuming that out-of-plane buckling does not occur in the beam and column, in numerical analysis, out-of-plane displacement will be restricted as shown in Figure (7).

As in the laboratory model loading is performed with up to a 3% drift. Therefore, 3% is considered a fracture criterion to determine the buckling in the

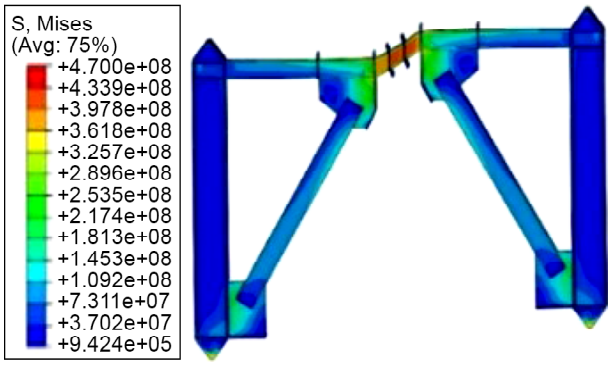

Figure 5. Numerical stress contour for Berman and Bruneau (2006) models.

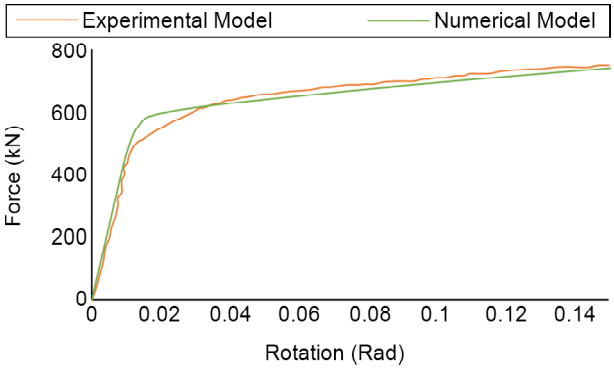

Figure 6. Numerical versus experimental results for Berman and Bruneau (2007).

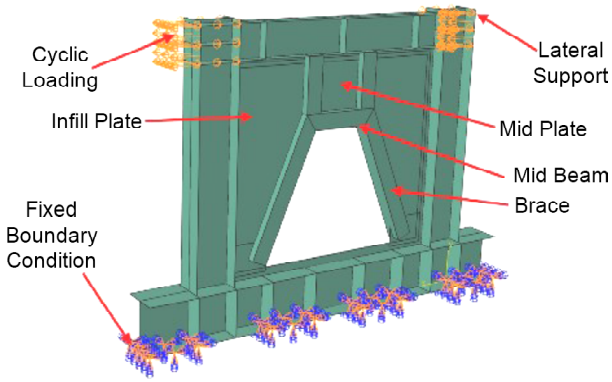

Figure 7. Modeling details of the W1.5-BP270-B1000.

infill plate and other members, loading continues beyond the capacity of the structure (up to 5% drift). In the experimental test, the loading is monotonic, but in the present study, to consider the effect of the cyclic loading on the structure, the loading protocol from the ATC-24 code (Council, 1992), is used. For cyclic loading Group 1 (Figures 8 to 11), the base model (SPW-0) is first loaded monotonically to determine the amount of yield displacement (δ_y). The cyclic loading protocol is introduced as: $\pm 0.4\delta_y$, $\pm\delta_y$, $\pm 2\delta_y$, $\pm 4\delta_y$, $\pm 8\delta_y$, $\pm 12\delta_y$, $\pm\delta_y$. In this proposed loading protocol, all cycles were applied twice, according to Figure (12).

Finally, cycles 6 and 7 were applied to ensure yielding and plastic deformations in the infill panel. The models were found to undergo a drift of 3% nearly in cycle 5. For Group 2 (Figures 14 ~19), a cyclic load was applied as $\pm 1.16\delta_y$, $\pm 1.4\delta_y$, $\pm 2.5\delta_y$, $\pm 5.5\delta_y$, $\pm 11\delta_y$, $\pm 16\delta_y$, and $\pm 22\delta_y$. According to Figure (13) cycles were implemented two times. For Figures (14) to (19), the base model Sa-LM was monotonically loaded to find the yield displacement δ_y as the base of the loading protocol.

An eccentrically braced frame (EBF) was employed in the models shown in Figures (15) to (19), whereas an SPSW was used in Figures (8) to (11). An opening size/structure height ratio in

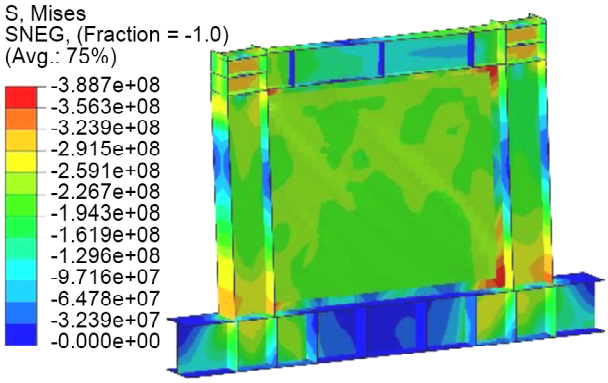

Figure 8. W1.5.

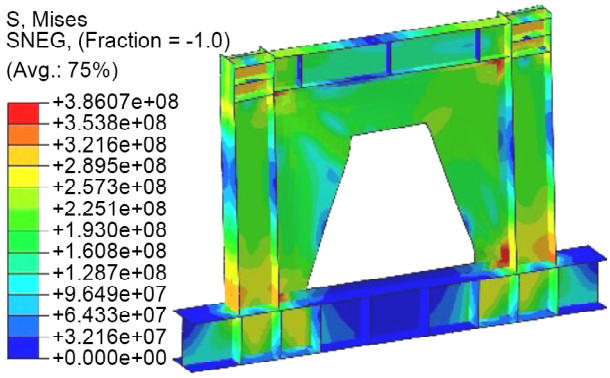

Figure 9. W1.5-P270.

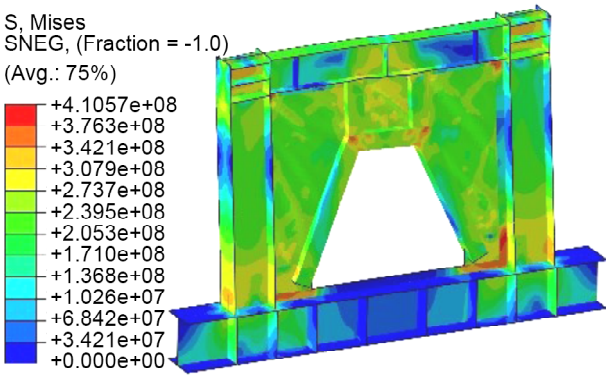

Figure 10. W1.5-BP270-B1000.

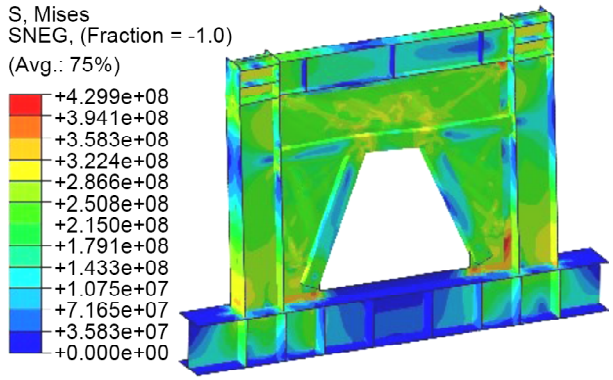

Figure 11. W1.5-EBP270-B641.

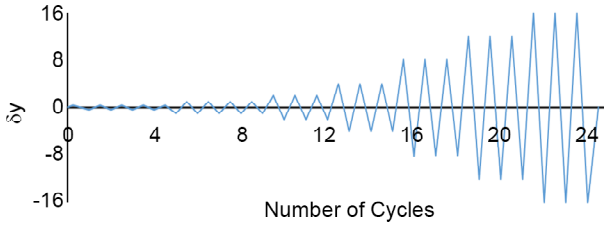

Figure 12. Cyclic loading for Group 1 models.

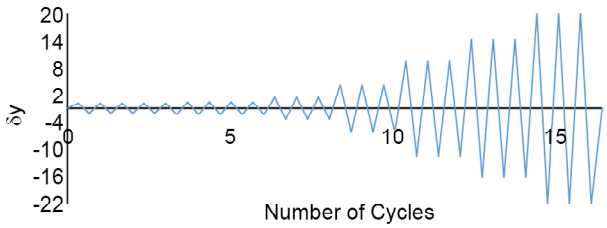

Figure 13. Cyclic loading for Group 2 models.

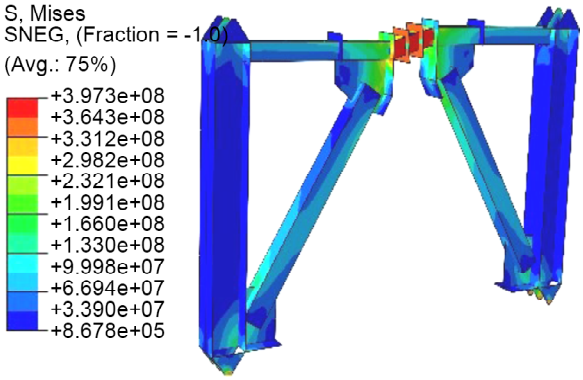

Figure 14. Sa-LM.

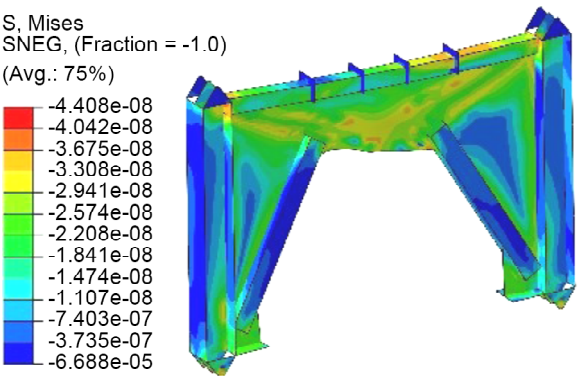

Figure 15. W8-LP8-P742-B1860.

Group 1 (Figures 9 to 11) was set to almost 73%. The opening size/structure height ratio in Group 2 was 69%, assumed to reduce inaccessibility. Hence, the openings were efficient in all the models and remarkably reduced accessibility limitations. According to the results (Group 1), in the 5th cycle, almost all models reach a 3% drift. The opening dimensions at the bottom and top of the steel plate are 850 mm and 400 mm, respectively, with a height of 710 mm and a 72.50 angle from the horizon (Figure 9). This prevents the formation of a symmetrical diagonal tension field in the steel plate, resulting in a noticeable local buckling at the left corner of the steel plate. Therefore, to control the buckling at the opening edges and to create suitable support for the formation of the tension field, it is recommended to use diagonal braces, as shown in Figures (10) and (11). Moreover, to develop the diagonal tension field in the infill plates, it is recommended to extend the middle beam to the columns in a symmetrical manner, as shown in Figure (11). Thus, in Table (1), the

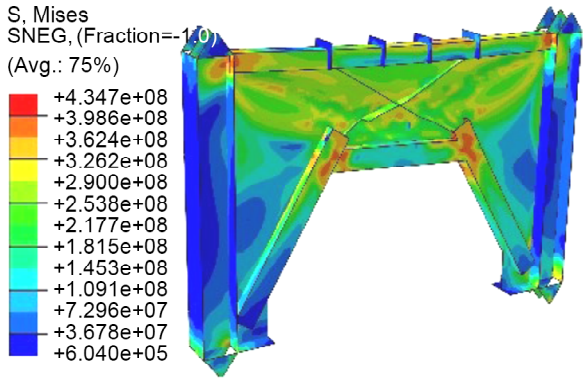

Figure 16. W8-LP8-BP739-B1780-Ds.

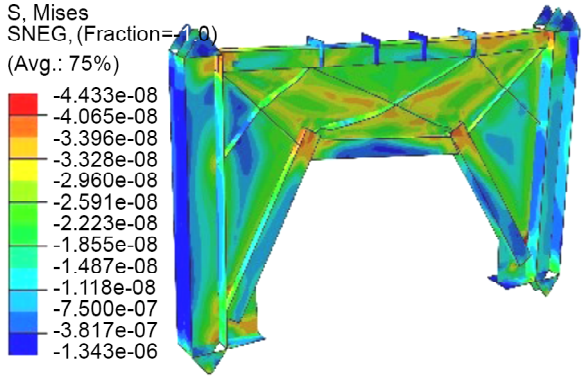

Figure 18. W8-LP8-BP742-B1700-3Ds.

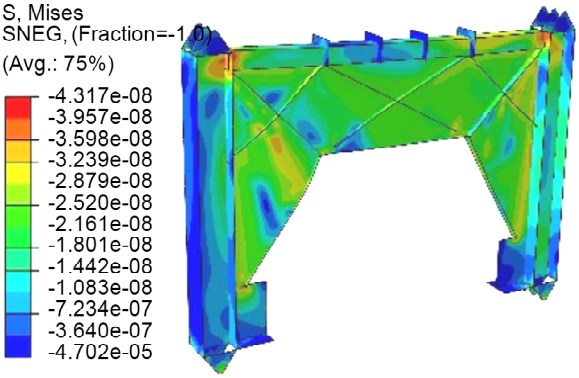

Figure 17. W8-LP8-P742- 3Ds.

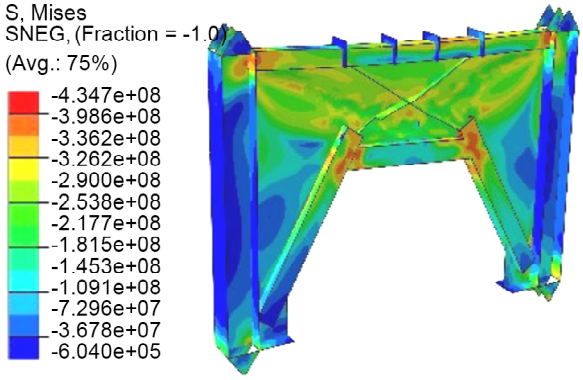

Figure 19. W8-LP8-BP739-B1780-3Ds.

Table 1. W8-LP8-P742-B1860.

Group	Model	Column	Beam	Steel Plate Thickness (mm)	Mid Plate Thicknes s (mm)	Height Mid Plate (mm)	Stiffener Thicknes s (mm)	Stiffener Width (mm)	Brace (mm)	Brace Length (mm)
Group 1	W1.5	170×150×15×15	140×100×10×10	1.5	-	-	-	-	-	-
	W1.5-P270	170×150×15×15	140×100×10×10	1.5	1.5	270	-	-	Box 80×80×8	-
	W1.5-BP270-B1000	170×150×15×15	140×100×10×10	1.5	1.5	270	-	-	Box 80×80×8	1000
	W1.5-EBP-B641	170×150×15×15	140×100×10×10	1.5	1.5	270	-	-	Box 80×80×8	641
Group 2	SA-LM	W310×143	152×150×16×6	-	-	-	-	-	-	-
	W8-LP8-P742-B1860	W310×143	152×150×16×6	8	8	742	-	-	-	1860
	W8-LP8-BP739-B1780-Ds	W310×143	152×150×16×6	8	8	739	10	60	191×178×11.8	1780
	W8-LP8-P742-3Ds	W310×143	152×150×16×6	8	8	742	8	60	-	-
	W8-LP8-BP742-B1700-3Ds	W310×143	152×150×16×6	8	8	742	8	60	160×160×11	1700
	W8-LP8-BP739-B1780-3Ds	W310×143	152×150×16×6	8	8	739	8	60	191×178×11.8	1780

geometric specifications of the numerical models are designed based on AISC (2016).

4. Failure Mechanism and Loading

Experimental models can often be loaded until the bearing elements of the structure fail. For numerical models, however, partial and total failure limits should be taken into account to discontinue the loading process based on the mechanical properties and load capacities of the elements. Total failure criteria often control the structural response (i.e., load displacement or moment rotation) and assume a sharp reduction in the load capacity as the failure limit. However, a partial failure limit occurs before the total failure and can involve brittle fractures (e.g., torsional failure of columns, beam shear connection failure, and fracture of a plate or plate connections to the frame) and ductile fractures (e.g., bolt failure, local buckling in the flange/web, and diagonal tension field development in steel plates). Such mechanisms, including yielding, failure, and buckling, reduce the strength of the overall response of the structural system. Hence, existing codes determine a limit for the sharp reduction in the overall structural response. A strength reduction larger than this limit would represent the ultimate capacity of the system in numerical models. For example, FEMA (2009) assumes a sharp strength reduction larger than 20% at an incremental step to represent the ultimate load capacity of the structure. For Group 1 (Sigariyazd et al., 2016), incremental loading in W1.5 and all the failure mechanisms, such as local buckling and tension field development in the steel plate, would be evaluated at a drift of 3%. In the desirable mechanisms, plastic stresses propagate first in the middle plate and then in the side plates. An increase in the load leads to a ductile failure, including the local buckling of the beam web or flange, the buckling of the steel plate, and the local buckling of the column, with the columns remaining elastic at the end. In general, the thickness of the steel plate should be optimized so that the moment transferred from the beam to the column does not induce plastic deformations in the column and does not prevent diagonal tension field development in the steel infill panel. In the models proposed by Berman and Bruneau (2007), Group 2 was loaded to a link beam rotation of 0.14 rad (a drift of 2%). Moreover, the failure criterion was conservative, and the ultimate capacity of real-life structures can be slightly larger than the reported values.

4.1. Cyclic Behavior

Cycle diagrams are one of the most important responses to assess the seismic bearing systems. In the cycle diagrams, the response of each proposed model is compared with the W1.5 model. According to the model W1.5-P270 diagram shown in Figure (20), the load-carrying capacity is decreased by 18% due to the presence of an opening, resulting in local buckling in the steel plate. In two models, namely W1.5-BP270-B1000 and W1.5-EBP270-B641, the addition of a beam between two braces leads to the formation of a diagonal tension field on the plate. In Figure (21), the strength is increased by about 17% at a 5% drift. Dissipated energy is a

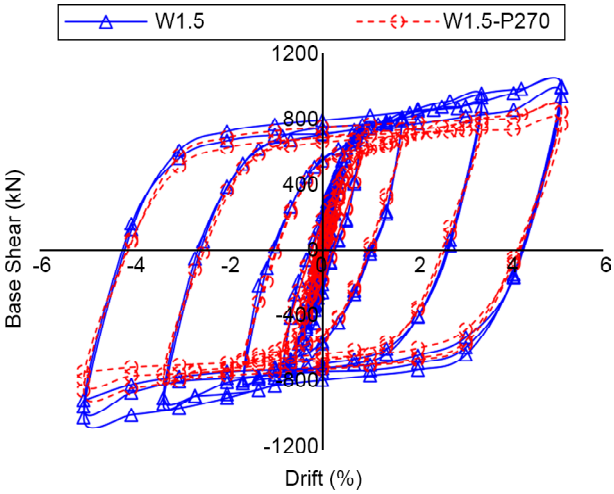

Figure 20. Load-drift response of the model W1.5.

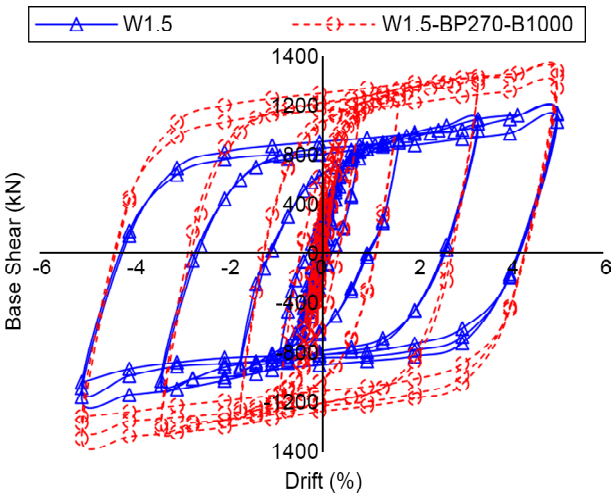

Figure 21. Load-drift response of the model W1.5-P270.

critical analysis outcome in determining the system's energy dissipation capability. The highest energy dissipation is related to the W1.5-BP270-B1000 model, which is 25% larger than that of the W1.5 model.

In Figure (22), the W1.5-EBP270-B641 model performs better than the other models in terms of all the studied responses, including the buckling mode of the infill plates, the rate of strength drops, the stability of cyclic response, and energy dissipating. Moreover, all the above-mentioned models have larger energy dissipation and stiffness than the W1.5 model. As the stiffness of the structure increases, the base shear also increases (Table 2). It is observed that by controll-ing the buckling of the steel plate, the amount of out-of-plate displacement becomes negligible.

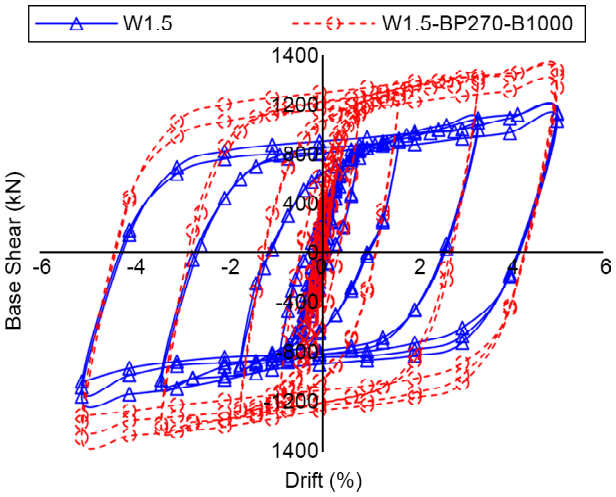

Figure 22. Load-drift response of the model W1.5-EBP270-B641.

In the Group 2 models, the height of the plate is 740 mm, and the height of the middle plate is approximately 30% of the frame span height. The purpose of the middle plate is to improve ductility and control local buckling at the connection point of the brace to the middle plate. Therefore, to control or reduce buckling in this area, the aim is to prevent local buckling using intermediate beams in the middle plate area. Additionally, by converting the global buckling of the plate into partial buckling and spreading the tension fields across the entire surface of the plate, ductility is consequently increased. With the placement of cross stiffeners, the middle plate cannot move freely under cyclic loading due to the connection of the beam to the middle plate (Maleki et al. 2024). Therefore, the likelihood of forming a diagonal tension field in this area increases under cyclic loading, producing spindle-shaped cycles. As shown in Figures (23) to (27), the models with cross stiffeners and

Table 2. Load-drift response of the model W1.5-EBP270-B641.

Model	$K_{initial}$ (kN/mm)	Energy Dissipation Coefficient (Drift 3%)	Out of Plane Displacement (mm)	Model Deforming
W1.5	229.4	1.93	45	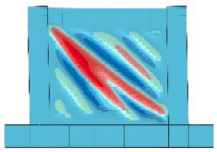
W1.5-P270	139.9	2.13	113	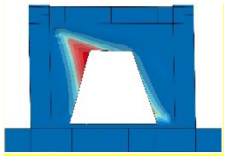
W1.5-BP270-B1000	260.5	2.54	26	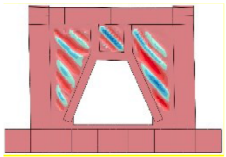
W1.5-EBP270-B641	229.8	2.08	19	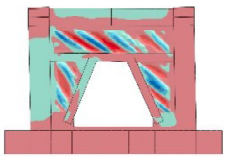

intermediate beams show increased stiffness and resistance parameters compared to models without stiffeners. However, these models still face ductility issues due to local buckling at the brace-to-middle plate connection, leading to a stiffness reduction in the compression. In all samples, the use of infill plates resulted in increased stiffness in both elastic and plastic stages.

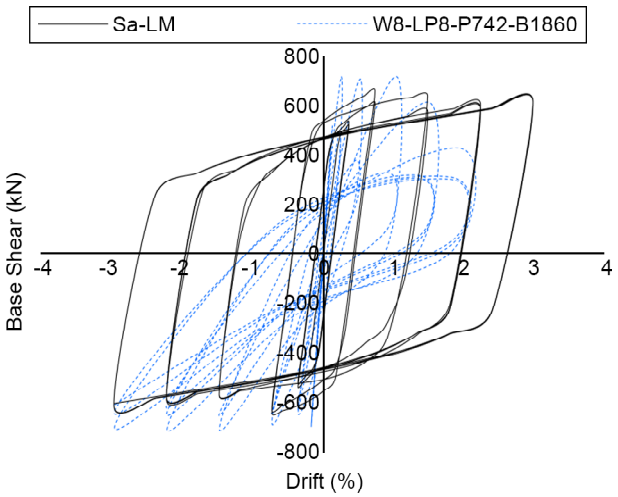

Figure 23. Load-drift response of the model.

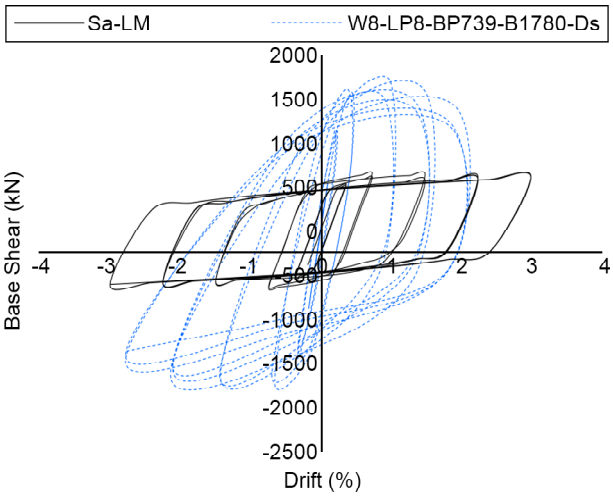

Figure 24. Load-drift response of the model.

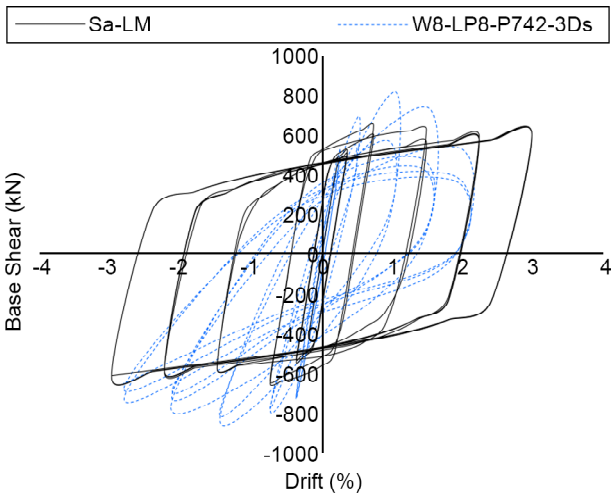

Figure 25. Load-drift response of the model.

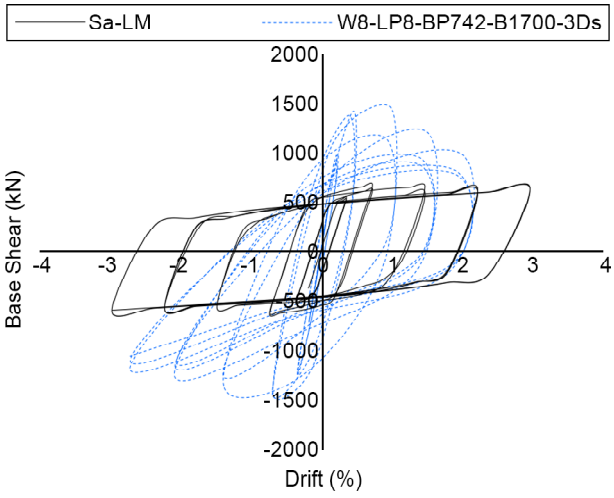

Figure 26. Load-drift response of the model.

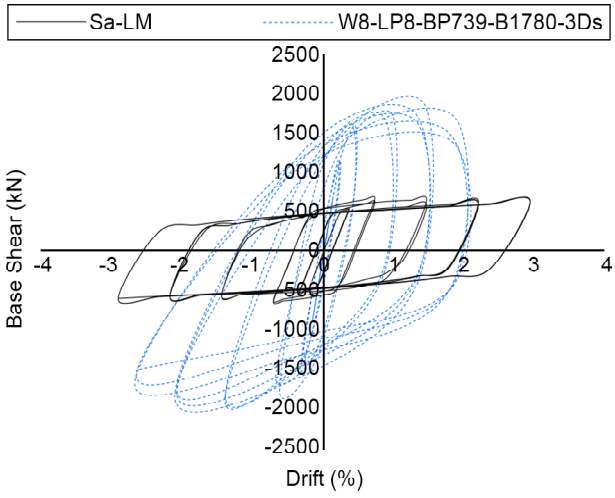

Figure 27. Load-drift response of the model.

4.2. Stiffness and Damping

The energy dissipation coefficient is a crucial parameter in assessing a system's energy absorption capacity. The method for calculating this parameter, as shown in Figure (28), follows the recommendations provided in (JGJ101-96) (Zhongming et al., 2009). Therefore, the energy dissipation coefficient $(\tilde{E})$ is calculated using Equation (5). In this equation, SCDA and SABC represent the areas of the upper and lower halves of the force-displacement hysteresis loop, respectively, while SOBE and SODF are the corresponding triangle areas in Figure (28). In other words, as the area of the hysteresis loops increases, the energy dissipation capacity of the structure also increases. The coefficients for each structure are determined using Equation (5) and presented in Table (3).

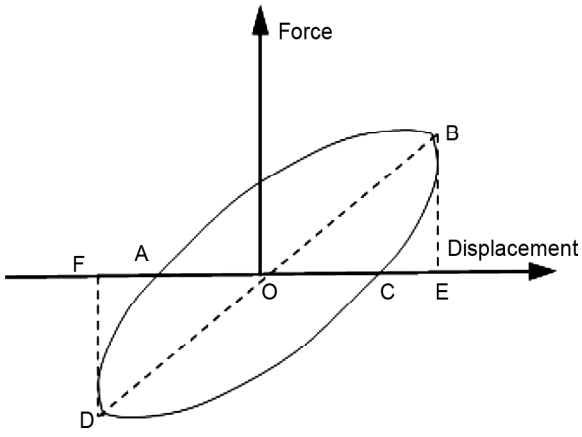

Figure 28. Load-displacement curve to calculate Energy.

The concept of viscous damping is typically applied to describe a structure's ability to dissipate energy within the elastic range. Energy dissipation occurs due to various mechanisms such as cracking, nonlinear response, interaction of non-structural elements, and soil-structure interaction. Elastic, viscous damping is a combination of all these energy dissipation mechanisms. In the 1930s and 1960s, Jacobsen proposed an approximate linear model to calculate viscous damping using a single degree of freedom (SODF) system subjected to sinusoidal loads. Later, Housner in 1956 and

Table 3. Summary of the results of the studied parameters of Group 2 models.

Model	$K_{initial}$ (kN/mm)	Energy Dissipation Coefficient (Drift 3%)	Out of Plane Displacement (mm)	Model Deforming
W8-LP8-P742-B1860	157.5	2.2	256	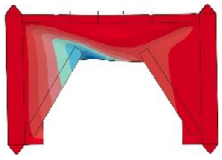
W8-LP8-BP739-B1780-Ds	209.8	1.54	99	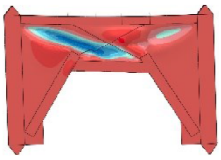
W8-LP8-P742- 3Ds	209.8	2.04	262	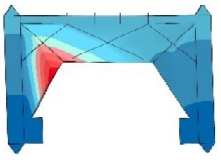
W8-LP8-BP742- B1700-3Ds	172.2	1.89	189	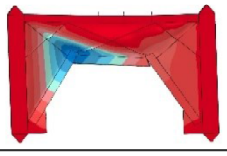
W8-LP8-BP739-B1780-3Ds	209.8	1.61	96	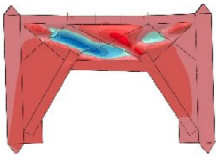

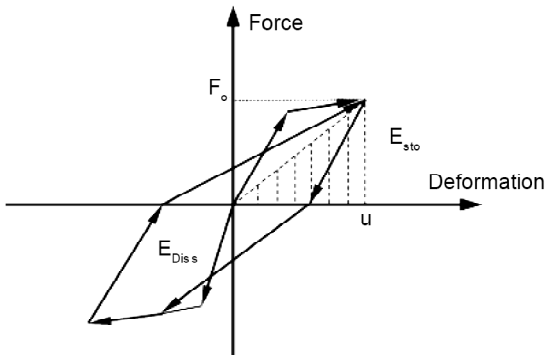

Figure 29. Load-displacement curve to calculate damping.

Jennings in 1964 conducted studies to expand the concept of cyclic systems. Generally, the viscous damping coefficient consists of two main parts. According to Equation (6), ξ_0 is the initial damping in the elastic range, and ξ_{hyst} is the viscous damping due to the system's nonlinear behavior (Blandon & Priestley, 2005), The energy stored in the elastic state is obtained using Equation (7), as shown in Figure (29). Finally, assuming the excitation frequency matches the natural frequency of the single degree of freedom structure (resonance condition), the energy dissipation (E_{Diss}) equals the enclosed hysteresis loop area (A_{hyst}) (see Equation (8)). Therefore, hysteresis damping is the ratio of E_{Diss} to the elastic strain energy (E_{sto}), as given by Equation (9).

$$\tilde{E} = \frac{S_{(ABC+CDA)}}{S_{(OBE+ODF)}} \tag{5}$$

$$\xi_{eq} = \xi_0 + \xi_{hyst} \tag{6}$$

$$E_{sto} = \frac{ku_o^2}{2} \tag{7}$$

$$E_{Diss} = A_{hyst} \tag{8}$$

$$\xi_{hyst} = \frac{1}{4\pi} \cdot \frac{E_{Diss}}{E_{sto}} = \frac{1}{2\pi} \frac{A_{hyst}}{F_o u_o} \tag{9}$$

According to Figure (30), for all models in Group G1, the damping parameter has increased compared to the W1.5 model. For models W1.5-BP270-B1000 and W1.5-EBP270-B641, at a drift of 1.7%, the damping parameters are 56% and 52%, respectively. As mentioned, the damping increases until the end of the elastic stage. However, after the first yield or local buckling in the inelastic stage, the damping decreases. In the proposed models, the reduction is due to the formation of irregular tension fields and overall buckling in the steel plate between the mid and main beams, as well as local buckling and joint failure at the top of the column.

In Figure (31), the damping parameter for each model is presented. As previously mentioned, the purpose of using intermediate beams was to improve the ductility parameter in the structural response. With loading and the formation of tension fields in the plate, the brace buckles at the connection to the middle plate in the compressive region, causing asymmetry in the structural response. As shown, an increase in the area under the curve leads to an increase in energy absorption and damping of the structure. Due to this asymmetry in the structural response, the damping and energy

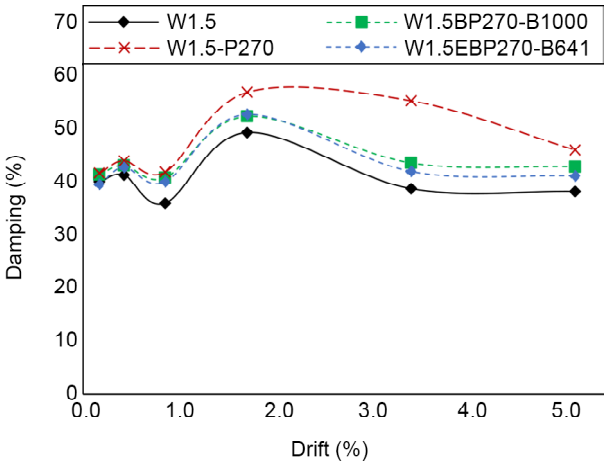

Figure 30. Damping ratios of Group 1.

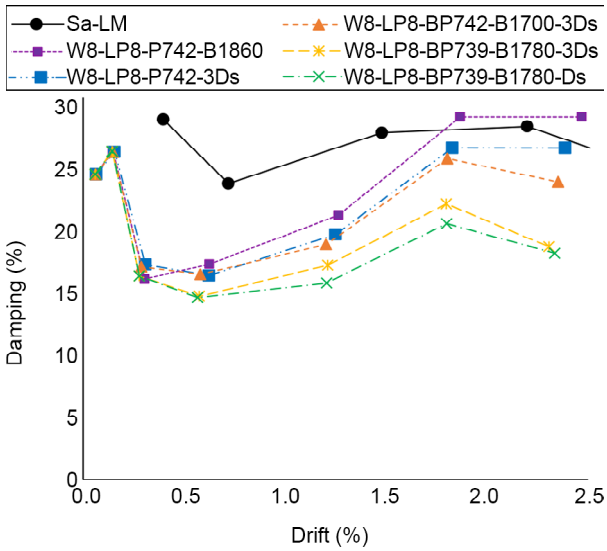

Figure 31. Damping ratios of Group 2.

parameters, as shown in Table (3), have decreased compared to the energy parameter for the baseline model Sa-LM, which is 2.23. Additionally, as observed for the modified models in Table (3), the use of an intermediate beam at the edge of the opening, compared to samples without an intermediate beam, has led to the partial formation of diagonal tension fields. The observed diagonal buckling does not change direction under reverse loading, preventing the reformation of the tension field perpendicular to the initial buckling direction (Breath Effecting). It is worth noting that, at the final loading stage, the steel infill plate experiences tension, causing some downward deflection of the beam. This can be one of the reasons for the improper formation of diagonal tension fields in these proposed models. Moreover, Table (3) specifies the maximum value and location of buckling separately, indicating that the maximum buckling occurs at the brace-to-beam connection on the middle plate in all models. Consequently, local buckling in the middle plate prevents the formation of tension fields, resulting in reduced capacity in the compressive region of the plate. Table (3) and Figure (31) show that the energy and damping values decrease, indicating the structure's ability to dissipate energy.

Figure (32) shows the stiffness degradation for Group 1 models. The maximum stiffness for the baseline sample is approximately 229 kN/mm. With the introduction of an opening in model W1.5-P270, stiffness decreases to 139 kN/mm. Additionally, in model W1.5-BP270-B1000, the stiffness is 186 kN/mm, where a link beam and braces extend from the connection plate to below the main beam.

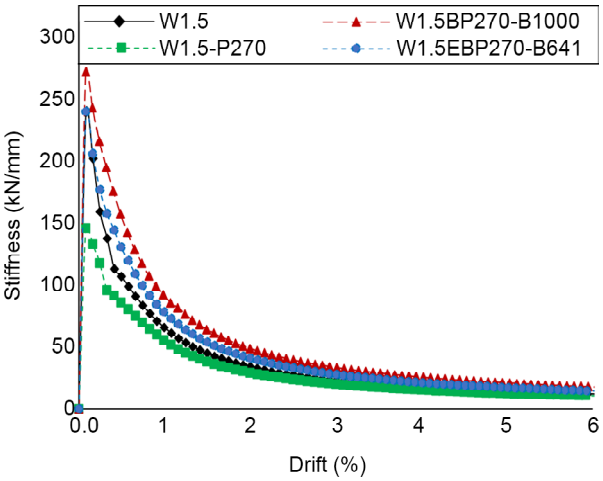

Figure 32. Stiffness deterioration of Group 1.

In Figure (11), it can be seen that the simultaneous presence of the intermediate beam and braces extending below the middle beam transforms the plate into regular geometric shapes, forming diagonal tension fields in the infill plate. In Group 2 models, as shown in Figure (33), the highest stiffness value is 272.2 kN for model W8-LP8-BP742-B1700-3Ds, while the lowest value is 209.8 kN for model W8-LP8-P742-3Ds. The difference between the two models is the presence of an intermediate beam, which increases stiffness by approximately 30% by stiffening the edge of the opening. In steel frames with eccentric braces, infill plates increase the stiffness and resistance of the system. The results show that the middle plate enhances structural resistance and stiffness.

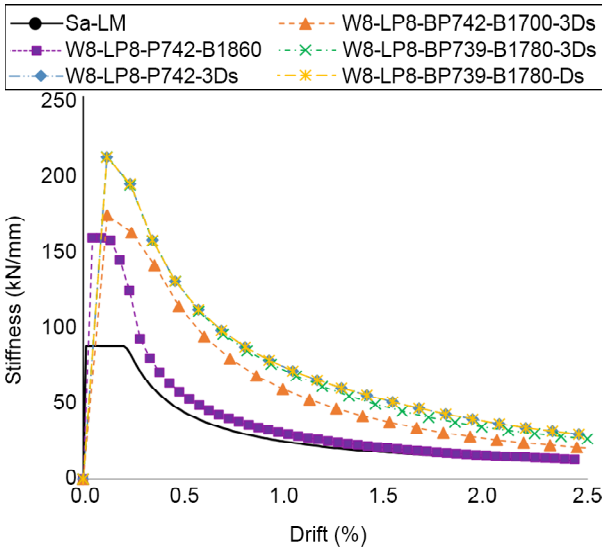

Figure 33. Stiffness deterioration of Group 2.

5. Conclusion

1. According to the proposed models, buckling occurs in steel plates by creating an opening, and the diagonal tension field is not formed completely, as observed in model W1.5-P270. To improve and control buckling behavior, eccentric bracing elements were used at the opening. In most numerical models, at the 3% drift, buckling occurs at the opening, and then the steel plate yields. As the loading increases and the drift reaches 5%, local flexural buckling is also observed in the column flange.
2. When the brace is connected to the main beam (W1.5-BP270-B1000) compared to a continuous middle beam connection form (W1.5-EBP270-

B641), the cyclic load-resisting capacity increases, and a diagonal tension field forms properly.

3. The highest capability in terms of energy dissipation and viscous damping relates to the W1.5-BP270-B1000 model. Energy dissipation increases by about 25% compared to the W1.5 base model.
4. Using infill plates in steel frames with eccentric braces increases the system's stiffness and resistance parameters. The results show that the middle plate is crucial for providing stiffness and enhancing structural resistance.
5. In the proposed models based on SPSW with openings, global buckling occurs in the steel plate, and diagonal tension fields do not fully form, as observed in model W1.5-P270. Eccentric braces were used at the openings to improve the behavior and control buckling. In most numerical models, buckling occurs at the openings at a drift of 3%, followed by the yielding of the steel plate.
6. In steel plates exhibiting shear behavior where complete diagonal tension fields cannot form, stiffeners prevent sudden resistance loss but do not significantly increase the overall structural stiffness.
7. The proposed system of using infill steel plates in EBF frames aims to enhance the performance of EBF systems and to develop the proposed model based on EBF systems. However, this approach did not show satisfactory performance based on the EBF system, unlike the developed model based on SPSW systems. Adding infill plates increases system stiffness, resulting in higher tensile stresses on the beam and creating a rupture mechanism at the beam-to-column connection at the top of the beam. Consequently, vertical boundary elements must resist these forces, leading to decreased resistance in the compressive region during cyclic behavior.

References

American Institute of Steel Construction. (2016). *Seismic Provisions for Structural Steel Buildings* (AISC 341-16).

Applied Technology Council. (1992). Guidelines for cyclic seismic testing of components of steel structures (ATC-24).

Berman, J. W., & Bruneau, M. (2007). Experimental and analytical investigation of tubular links for eccentrically braced frames. In *Engineering Structures*, *29*(8), 1929-1938. doi: 10.1016/j.engstruct.2006.10.012

Blandon, C. A., & Priestley, M. J. N. (2005). Equivalent viscous damping equations for direct displacement based design. *Journal of Earthquake Engineering*, *9*(2), 257-278. doi: 10.1142/S1363246905002390

Dubina, D., & Dinu, F. (2014). Experimental evaluation of dual frame structures with thin-walled steel panels. *Thin-Walled Structures*, *78*, 57-69. doi: 10.1016/j.tws.2014.01.001

Es, F., Hoseinzadeh, M., & Hosseinzadeh, Y. (2023). Experimental and numerical investigation of a new type of steel plate shear wall with diagonal tension field guiding stiffeners. *Journal of Building Engineering*, *76*, 107181. doi: 10.1016/j.jobe.2023.107181

Farrokhi, A. A., Rahimi, S., Beygi, M. H., & Hoseinzadeh, M. (2022). Numerical finite element study of a new perforated steel plate shear wall under cyclic loading. *Earthquakes and Structures*, *22*(6), 539-553.

Farzampour, A., Laman, J. A., & Mofid, M. (2015). Behavior prediction of corrugated steel plate shear walls with openings. *Journal of Constructional Steel Research*, *114*, 258-268. doi: 10.1016/j.jcsr.2015.07.018

FEMA. (2009). *Quantification of Building Seismic Performance Factors* (FEMA P695).

Ghosh, S., & Kharmale, S. B. (2010). Research on steel plate shear wall: Past, present and future. In *Structural Steel and Castings: Shapes and Standards, Properties and Applications*.

Jin, S., & Bai, J. (2019). Experimental investigation of buckling-restrained steel plate shear walls with inclined-slots. *Journal of Constructional Steel Research*, *155*, 144-156. doi: 10.1016/j.jcsr.2018.12.021

Maleki, A., Khalili Sarbangoli, R., & K. Badri, R. (2024). Evaluation of cyclic behavior of steel frame with infill plate and eccentric brace. *9th International Conference on Seismology and Earthquake Engineering*, Tehran, Iran

Ministry of Housing and Urban-Rural Development of the People's Republic of China. (2009). Code for seismic design of buildings (GB 50011-2001).

Nassernia, S., & Showkati, H. (2017). Experimental study of opening effects on mid-span steel plate shear walls. *Journal of Constructional Steel Research*, 137, 8-18.

Pachideh, G., Gholhaki, M., & Saedi Daryan, A. (2019). Analyzing the damage index of steel plate shear walls using pushover analysis. *Structures*, *20*, 437-451. doi: 10.1016/j.istruc.2019.05.005

Paslar, N., Farzampour, A., & Hatami, F. (2020). Infill plate interconnection effects on the structural behavior of steel plate shear walls. *Thin-Walled Structures*, *149*, 106621.

Ras, A., & Basri, H. (2024). Enhancing steel building dynamic performance under cyclic loadings using plate steel shear panels. *Asian Journal of Civil Engineering*, 1-10.

Roudsari, S. S., Soleimani, S. M., & Hamoush, S. A. (2021). Analytical study of the effects of opening characteristics and plate thickness on the performance of sinusoidal and trapezoidal corrugated steel plate shear walls. *Journal of Constructional Steel Research*, *182*, 106660.

Sahoo, D. R., Sidhu, B. S., & Kumar, A. (2015). Behavior of unstiffened steel plate shear wall with simple beam-to-column connections and flexible boundary elements. *International Journal of Steel Structures*, *15*(1), 75-87. doi: 10.1007/s13296-015-3005-5

Sigariyazd, M. A., Joghataie, A., & Attari, N. K. A. (2016). Analysis and design recommendations for diagonally stiffened steel plate shear walls. *Thin-Walled Structures*, 103, 72-80. doi: 10.1016/j.tws.2016.02.008

Wang, M., Duan, H., & Shi, G. (2024). Cyclic behavior of improved low-yield point steel plate shear walls with T-shaped stiffeners. *Journal of Building Engineering*, 109997.

Wang, M., Shi, Y., Xu, J., Yang, W., & Li, Y. (2015). Experimental and numerical study of unstiffened steel plate shear wall structures. *Journal of Constructional Steel Research*, *112*, 373-386.

Yang, Y., Mu, Z., & Zhu, B. (2022). Study on steel plate shear walls with diagonal stiffeners by cross brace-strip model. *Structural Engineering and Mechanics*, *84*(1), 113-127.

Zarrinkolaei, F. A., Naseri, A., & Gholampour, S. (2021). Numerical assessment of effect of opening on behavior of perforated steel shear walls. *Journal of Constructional Steel Research*, *181*, 106587.